FACULTY
OF SCIENCE

All solid state single-shot Dispersion scan (D-Scan) for ultrashort laser pulses

Shekhar Jadhav

Thesis submitted for the degree of Master of Science
Project duration: 8 months, 60 hp

Supervised by Chen Guo and Cord L Arnold

Department of Physics
Division of Atomic Physics
May 2019

Abstract

Ultrashort laser pulses play an important role in many applications in science and technology, from attosecond science to time resolved spectroscopy and material processing. For applications of ultrashort laser pulses, it requires a complete characterization of the electric field of the pulse, which includes both phase and amplitude of the electric field. The characterization of ultrashort laser pulses is very challenging, since we do not have a detector fast enough to measure electric field variations on short time scales such as femtoseconds. A novel characterization technique for ultrashort laser pulses, the dispersion scan (d-scan), was recently developed in Lund.

Here, a new compact single-shot version of the d-scan called Single-Shot d-scan (Si-scan) was developed, to extend the characterization technique to broader spectral range and longer durations. This technique employs a Transverse Second Harmonic Generation (TSHG) crystal which introduces dispersion as well as generating the second harmonic, resulting in a D-scan trace, i.e. SHG spectrum as a function of dispersion. The spectral phase can be retrieved from the D-scan trace by using a phase retrieval algorithm. Within the course of this work, the dispersion properties of the TSHG crystal were measured by using white-light spectral interferometry. A compact imaging spectrometer to measure the Si-scan trace by using the cross Czerny-Turner imaging spectrometer technique, which has very low astigmatism, was build. D-scans recorded with the new system are presented.

Acknowledgement

First of all, I would like to thank Anne L'Huillier and Cord Arnold for proposing this exciting project and giving me an opportunity to be part of it.

I would like to heart-fully thank my Supervisors Chen and Cord. Both of you were great supervisors and guide, who helped me a lot during my thesis, from planning to execution. Once again thanks a lot Chen for sharing your vast experience and clearing all my stupid doubts. And Cord, even though you were quite busy, you always had time for me to answer my questions and help me out with my problems during the thesis, and I am thankful for it. I couldn't have asked any better supervisors than both of you.

I had an amazing time at the Atto group and I am thank-full to each and everyone for integrating me into this group. Thanks a lot to Neven, Jan, Anna, Yu-Chen, David, Fabian, Lana, Ivan, Jasper, Sara, Emma, Hugo Laurell, Hampus, Hugo Dacasa Pereira, Helene, Jan Vogelsang, Alexandre, Maria, Simon. Thanks a lot, Åke for helping me set up the computer and Anne Petersson for helping me out with the registration.

Time to thank my Photonics buddies, I would like to thank Saskia for the valuable suggestions and discussions (you were the best lab partner). Thanks to Lisa and Armand for all the discussions and for motivating me during the thesis. Thanks to all my physics friends for the support which includes Ian, Javier, Robin, Jess, Erik, Max, Frans and Maitane.

Finally, I would like to express my gratitude to my family, Linnea, Anna and Linnea's family for all the support and encouragement throughout my masters.

Popular science summary

The human eye can clearly observe movements as fast as around 0.1 seconds long, but how can we observe the movement that is way too fast for the human eye? For example you can barely read any labels from a really fast moving formula 1 car, illustrated in figure (1a). however if we use a camera which can act faster than the human eye, we can capture the images of the moving object. When a camera takes a picture, it records all the light reaching the detector during the exposure time. To acquire a very sharp image we need a short flash of light which has a shorter duration than the motion. The shorter the light pulses, the faster the movements that can be observed, such as an acquired sharp image in figure (1b). Similarly, the movement of electrons around an atomic nucleus is on the timescale of attosecond (10^{-18} s), hence we need an attosecond light pulse to observe their motion. Thus, the development of such short light sources is essential for observing the fast motions.

Ultrashort laser pulses play an important role in many applications, such as laser eye surgery, microscopy, data storage etc. Since ultrashort laser pulses are artificially created, even shorter pulses are not available to measure them, so the pulses themselves have to be used. We further develop a recent technique called Dispersion scan (D-scan) to measure the duration of ultrashort laser pulses [1].

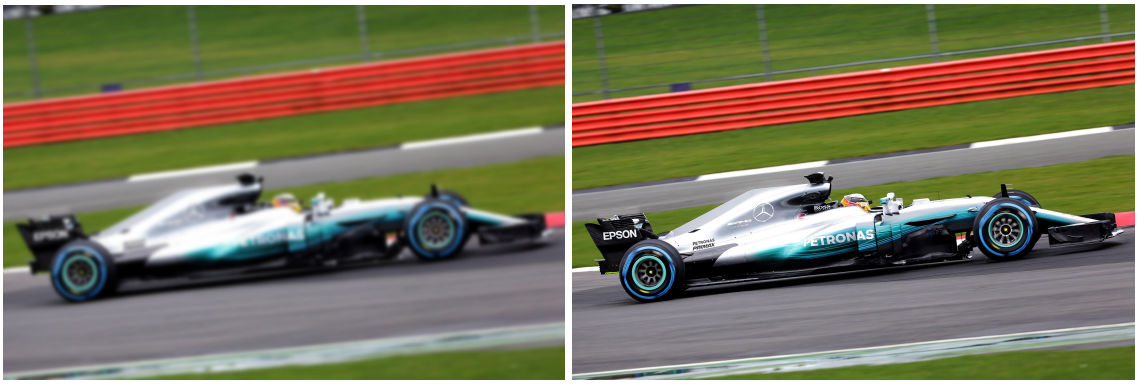

(a) Blurred image. (b) Sharp image.

Figure 1: Short flash of light pulse used to capture sharp image (b), and you can clearly read the text on image (b) compared to image (a). Image Source: [2]

Contents

List of Figures

Abbreviations

D-Scan	Dispersion Scan
FWHM	Full Width at Half Maximum
IR	Infrared
GDD	Group Delay Dispersion
GVD	Group Velocity Dispersion
MIIPS	Multiphotn Intrapulse Interference Phase scan
MIR	Mid-infrared
MPI	Multi Photon Ionization
OSA	Optical Spectrum Analyzer
SH	Second Harmonic
SHG	Second Harmonic Generation
Si-scan	Single shot D-scan
SPM	Self Phase Modulation
TSHG	Transverse Second Harmonic Generation
YAG	Yttrium Aluminium Garnet

1 Introduction

Intense ultrashort laser pulses in the femtosecond regime (1fs = 10^{-15} s), have become irreplaceable tools in the field of ultrafast optics and also in the fields of strong-field physics and attosecond science. Utilizing these short pulses for our experiments is extremely challenging; hence, we need a precise, convenient and easy-to-use characterization technique which is direct and intuitive and provides features of the pulse [3].

Throughout the years, several characterization techniques have been developed, for example Self-Referenced Spectral Interferometry (SRSI) [4], spectral phase interferometry for direct electric field reconstruction (SPIDER) [5], frequency-resolved optical gating (FROG) [6] and their multiple variants. These above methods are based on interferometric splitting and rather complicated. Furthermore, it is difficult to characterize the pulses in the temporal domain because it is often limited by the temporal profile, especially for shorter pulses in the femtosecond range.

Characterization of the pulses in a more controlled way has recently been developed based on manipulating the spectral phase. Some of the techniques which manipulate the spectral phase are chirp scan, multiphoton intrapulse interference (MIIPS) [7] and D-scan [1].

The characterization of ultrashort laser pulses is very challenging, in particular for few-cycle pulses, i.e. pulses for which the envelope encloses just a few oscillations of the electric field. The d-scan is based on the idea that the shape of the second-harmonic spectrum of an ultrashort pulse depends on the spectral phase of the fundamental spectrum. A d-scan trace consists of recording the second harmonic spectrum against a known variation of the spectral phase. In practice, one often moves wedges through the fundamental beam in order to introduce dispersion and to change the spectral phase. The spectral phase of the fundamental pulse can be obtained from the measured d-scan trace by solving an inverse problem iteratively.

It is difficult to characterize pulses with low repetition rates using a regular d-scan setup, since the shot-to-shot fluctuations would lead to absurd d-scan results by scanning the glass wedges. To characterize the low repetition pulses we need a single shot d-scan. For shorter laser pulses (< 10 fs) the single shot d-scan has been demonstrated [8]. But for longer pulses it is still not established, hence we need a different approach to achieve single shot d-scan for longer pulses.

1.1 Aim and Outline

The focus of the thesis is on developing a new compact single-shot characterization technique for ultrashort laser pulses, called Si-scan with the goal of extending the technique to broader spectral range and longer pulse durations (>20 fs). This technique employs a random phase matching Transverse Second Harmonic Generation (TSHG) crystal which introduces dispersion as well as generating SH in the transverse direction. The result is a Si-scan, i.e. the second harmonic spectrum recorded against the controlled manipulation of the spectral phase (through the dispersion of the crystal). The spectral phase of the pulse can be retrieved from the Si-scan trace by using a phase retrieval algorithm.

In the course of this work, the dispersion properties of the TSHG crystal were measured through white light interferometry. Knowledge of the dispersion of the crystal is essential for reliable retrieval.

Second, a compact imaging spectrometer using the cross Czerny-Turner geometry, which has really low astigmatism, was built. The Si-scan technique was implemented using the compact imaging spectrometer and the TSHG crystal. Based on the developed Si-scan, d-scan traces from a Titanium Sapphire chirped pulse amplification (CPA) laser were recorded and the pulses were retrieved.

Finally, I contributed to building a second d-scan setup for pulses from a Yb doped CPA laser. That work concentrated on generating efficient white-light from a YAG crystal in order to have a broadband source for testing the d-scan.

2 White-light spectral interferometry to calculate the dispersion of a material

2.1 Theory

White light spectral interferometry also known as spectral interferometry in short (by employing a high-resolution spectrometer to the interferometer), can be used to measure the dispersion of a material. It provides accurate and physically intuitive information of what happens to the pulses on transmission through a medium. Spectral interferometry is the measurement of the interference spectrum of a known and an unknown pulse. From the information you can retrieve the characteristics of an unknown pulse [9, 10].

The superposition principle of light gives rise to interference between two waves. Let us consider two ultrashort laser pulses: the known/reference pulse $E_1(\omega)$ and the unknown $E_2(\omega)$,

$$E_1(\omega) = |E(\omega)|exp(i\phi_1(\omega)) \tag{1}$$

$$E_2(\omega) = |E(\omega)|exp(i\phi_2(\omega))exp(i\omega\tau) \tag{2}$$

where $E(\omega)$ is the spectral amplitude, $\phi_1(\omega)$ and $\phi_2(\omega)$ are the phases of the known and unknown pulses respectively, and τ is the delay. Both pulses have an equal amplitude, since we use a 50/50 beam splitter in a Mach-Zehnder interferometer to split the source. The delay (τ) we introduce between two pulses leads to the phase term ($\omega\tau$) in $E_2(\omega)$. Let $\varphi(\omega)$ (i.e. phase difference between two pulses ϕ_2-ϕ_1) be the phase introduced by the material in one of the arms. The measured interference spectrum is a power spectrum $S_{int}(\omega)$,

$$S_{int}(\omega) = |E_1(\omega) + E_2(\omega)|^2 \tag{3}$$

$$S_{int}(\omega) = 2|E(\omega)|^2 + |E(\omega)|^2 e^{i\varphi(\omega)} e^{i\omega\tau} + |E(\omega)|^2 e^{-i\varphi(\omega)} e^{-i\omega\tau} \tag{4}$$

which is the interference spectrum between the known and unknown pulse. The fringe spacing depends on the phase difference $\varphi(\omega)$ and the time delay τ as shown.

$$S_{int}(\omega) = 2|E(\omega)|^2(1 + cos(\varphi(\omega) + \omega\tau)) \tag{5}$$

2.2 Experimental Setup and Procedure

We use a Mach-Zehnder interferometer setup to interfere the reference pulse and the unknown pulse (through the material) with a delay as shown in figure (2). In figure 2 beam splitter 1 splits the beam from the source, where material dispersion is introduced in one arm and in the other arm a delay stage controls the time delay between the pulses. Beam splitter 2 combines both pulses, which leads to spectral interference. This is observed by an Optical Spectrum Analyzer (OSA) with a resolution of 0.1 nm at a range of 55 nm.

The source used in the experiment was a supercontinuum laser source with a wavelength range of 450-1800 nm, a pulse duration of around 450 fs and a max pulse energy of 50 nJ.

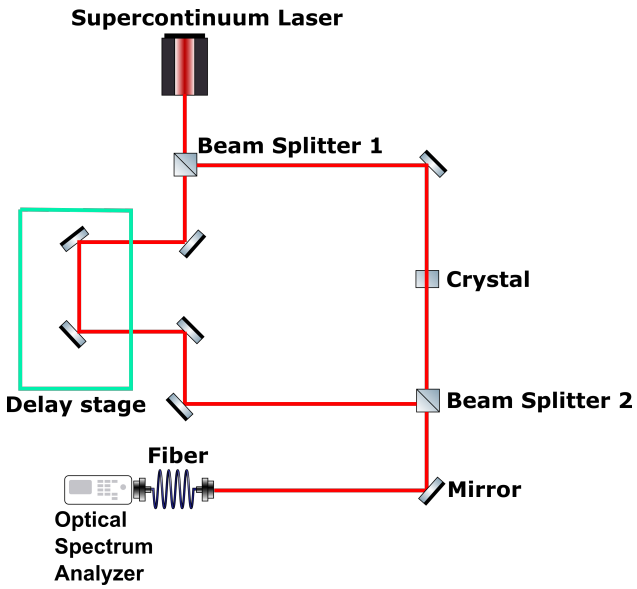

Figure 2: Mach–Zehnder interferometer with a white light source. Beam splitter 1 splits the source into two and Beam splitter 2 combines the reference pulse and unknown pulse through material which gives rise to spectral interference. A delay stage is used to control the time delay (τ) between the two pulses.

After the beam path in both arms is matched, the delay stage can be tuned to find spectral fringes. The delay is varied until clear fringes can be seen. The fringes should not be too dense though, to ensure good data sampling for proper spectral phase retrieval.

From the spectral interference as shown in equation (5), we know the delay τ and spectral phase (φ (ω)) introduced by the material is unknown. To retrieve the phase introduced by the material, which provides the dispersion of the material, the retrieval procedure will be discussed in the following section (2.2.1) phase extraction algorithm.

2.2.1 Phase extraction algorithm

The phase extraction algorithm consists of a series of steps, that can be summarized as follows:

1. Fourier transform the spectral interference pattern to the time domain as shown in equation (6).

$$\mathrm{F}\{\mathrm{S}_{int}(\omega)\} = F\{2|E(\omega)|^2\} + F\{|E(\omega)|^2 e^{i\varphi(\omega)} e^{i\omega\tau}\} + F\{|E(\omega)|^2 e^{-i\varphi(\omega)} e^{-i\omega\tau}\} \quad (6)$$

2. In the time domain we observe two sidebands as shown in equation (7) at $+\tau$ and $-\tau$, filter the sideband with positive delay ($+\tau$) using a super Gaussian filter.

$$\mathrm{F}\{\mathrm{S}_{int}(\omega)\} = F\{2|E(\omega)|^2\} + F\{|E(\omega)|^2 e^{i\varphi(\omega)}\} \circledast \delta(t-\tau) + F\{|E(\omega)|^2 e^{-i\varphi(\omega)}\} \circledast \delta(t+\tau) \quad (7)$$

3. After filtering the sideband, inverse Fourier transform it to the spectral domain, to obtain the spectral phase of the unknown pulse i.e. the phase introduced by the material.

4. Curve fit the spectral phase to obtain the second order dispersion (GDD/GVD) of the material.

We perform a Taylor series expansion of the phase term around the central frequency ω_o shown in equation (8), where ϕ_o is the absolute phase, ϕ'_o is Group Delay (GD), and ϕ''_o is the Group Delay Dispersion (GDD).

$$\phi(\omega) = \phi_o + \phi'_o(\omega - \omega_o) + \frac{1}{2!}\phi''_o(\omega - \omega_o)^2 + \frac{1}{3!}\phi'''_o(\omega - \omega_o)^3 + ... \quad (8)$$

$$\text{where } \phi_o = \phi(\omega_o),\ \phi'_o = \frac{\partial\phi(\omega)}{\partial\omega}\ at\ \omega = \omega_o$$

$$\phi''_o = \frac{\partial^2\phi(\omega)}{\partial\omega^2}\ at\ \omega = \omega_o$$

2.3 Results & Observations

2.3.1 Background calibration

Both (reference and unknown) beams travel through two different arms. The pulses may accumulate a phase difference due to coatings on various optical elements in the arms, so we need to measure the dispersion experienced by the pulses due to coatings; hence, we can calibrate the spectral interferometer for dispersion measurements.

In the figure 3, we follow the steps from the phase extraction algorithm (section 2.2.1) and obtain the GDD due to coatings on optical elements by fitting the spectral phase, which was 2.59 fs^2 at 800 nm. The spectral phase is quite linear as shown in figure 3(d), but still there is low second order dispersion due to the coatings.

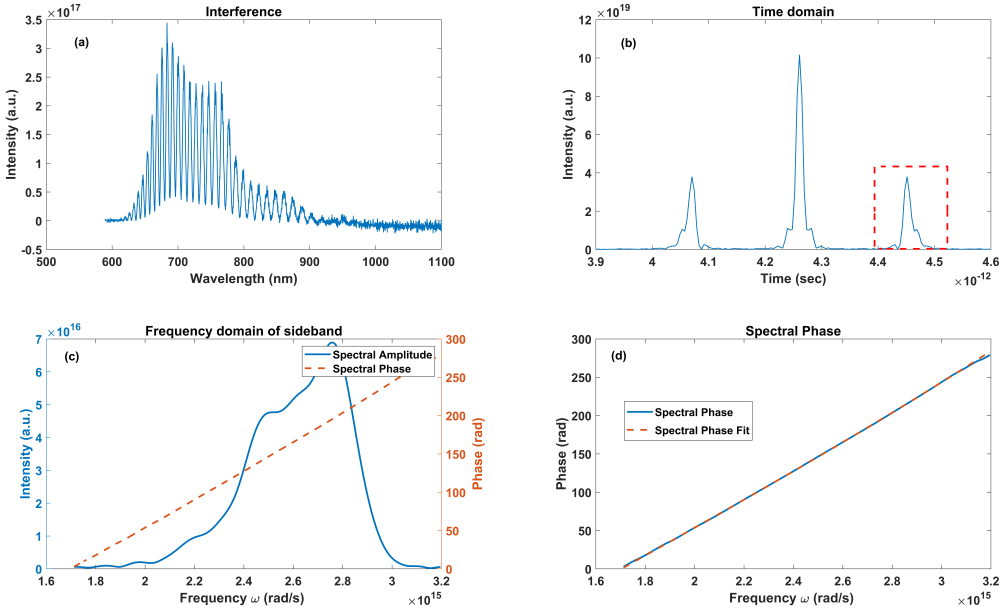

Figure 3: Dispersion measurement of coatings on optical elements in two arms, (a) Spectral interference pattern between pulses in two arms, (b) Time domain of spectral interference, filtering of positive delay in the time domain, which is marked in the red square (c) Inverse Fourier transforming the filtered sideband back to the spectral domain, blue plot curve shows the spectral amplitude of sideband and the red curve shows the spectral phase of the sideband, (d) Curve fitting of the spectral phase to obtain the GDD due to coatings, the blue curve shows the spectral phase of the sideband and the red curve shows the fitting of the spectral phase.

2.3.2 Dispersion measurement of fused silica

To validate the dispersion measurements, we measured the dispersion of a known material (fused silica). As shown in the figure (4), by the curve fitting of spectral phase of the sideband, the GVD obtained was 36.76 fs^2/mm (after calibration) at 800 nm, compared to the standard value of 36.16 fs^2/mm at 800 nm [11], our measured GVD was quite accurate.

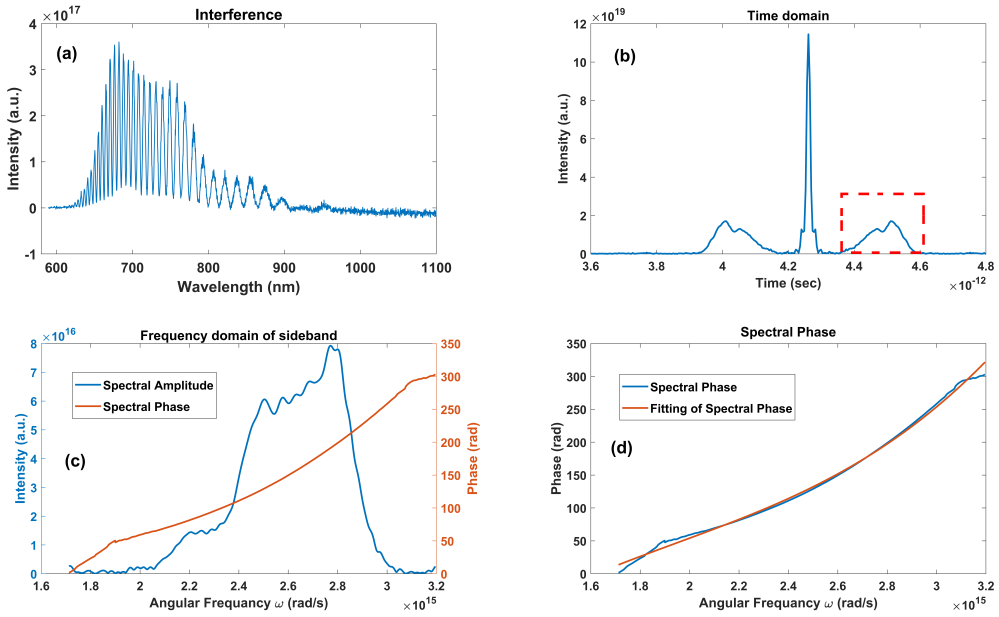

Figure 4: Dispersion measurement of fused silica of 6.35mm thickness, (a) Spectral interference pattern between pulses in two arms, (b) Time domain of spectral interference, filtering of positive delay in the time domain, which is marked in the red square (c) Inverse Fourier transforming of the filtered sideband back to the spectral domain, the blue plot curve shows the spectral amplitude of the sideband and the red curve shows the spectral phase of the sideband, (d) Curve fitting of the spectral phase to obtain the GVD of the fused silica, the blue curve shows the spectral phase of the sideband and the red curve shows the fitting of the spectral phase.

2.3.3 Dispersion measurement of unknown TSHG crystal

Figure (5) shows the interference spectrum of an unknown TSHG crystal in horizontal polarization, which is used in our characterization technique and will be discussed later. From figure 5 (a) we can observe that the fringes are very dense, this is due to large delay. To resolve these fringes for proper spectral phase retrieval we need a spectrometer with

sufficiently high resolution.

From the curve fitting of the spectral phase of the sideband figure 5 (d), the dispersion (GVD) of the TSHG crystal for horizontal polarization was found to be 480 fs^2/mm (after calibration) at 800 nm. Similarly, this was measured for vertical polarization, and the GVD was found to be 420 fs^2/mm (after calibration) at 800 nm.

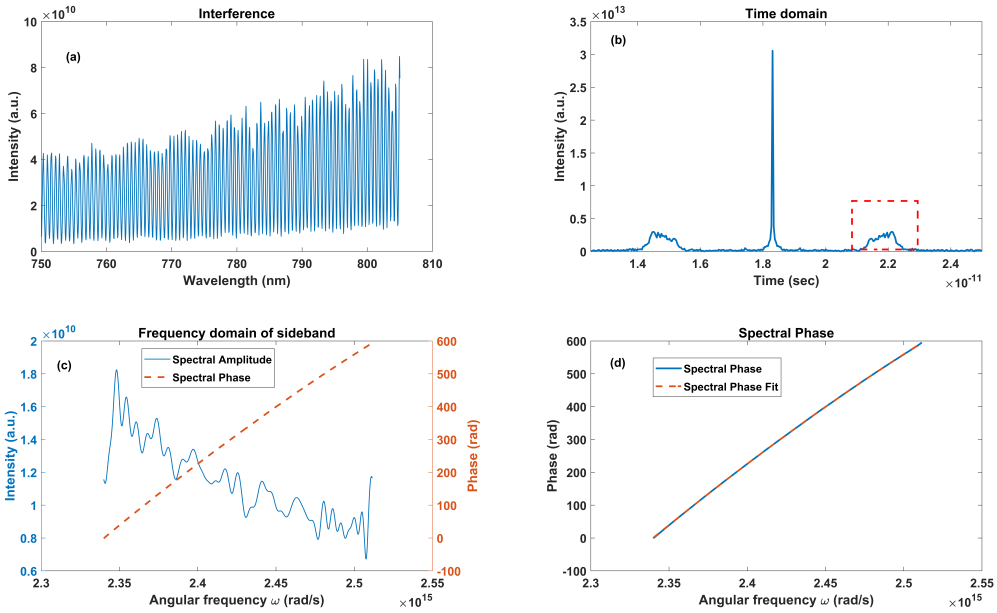

Figure 5: Dispersion measurement of unknown TSHG crystal in horizontal polarization of 10mm thickness, (a) Spectral interference pattern, (b) Time domain of spectral interference, filtering of positive delay in the time domain, which is marked in the red square (c) Inverse Fourier transform of the filtered sideband back to the spectral domain, the blue plot curve shows the spectral amplitude of the sideband and the red curve shows the spectral phase of the sideband, (d) Curve fitting of the spectral phase to obtain the GVD of the TSHG crystal in the horizontal direction, the blue curve shows the spectral phase of the sideband and the red curve shows the fitting of the spectral phase.

2.4 Conclusion

Large delays lead to dense fringes. In order to resolve the spectral fringes, the measurement requires a spectrometer with high resolution in order to resolve the fringes and filter the sideband.

White-light spectral interferometry has shown to be a powerful tool for accurately measuring the dispersion properties of optical components. We have measured the GVD

of an unknown TSHG crystal which was around 480 fs^2/mm. This is quite high and would be helpful in characterizing pulses with broader spectral range and longer durations.

3 Compact Imaging Spectrometer

3.1 Theory

3.1.1 Crossed Czerny-Turner imaging spectrometer

The crossed Czerny-Turner imaging spectrometer is very compact and astigmatism free [12]. In this work, we modified the spectrometer in the way that the astigmatism is compensated by a cylindrical lens, avoiding otherwise highly restricted positions of the components, so that it is easier to align and has better image quality over the whole field. The beam enters through the aperture/mask as shown in figure 6 and it is collimated by concave mirror 1 onto the grating, which then diffracts the beam into different angles according to the colour and reflects it onto concave mirror 2 which focuses the beam into a CCD camera.

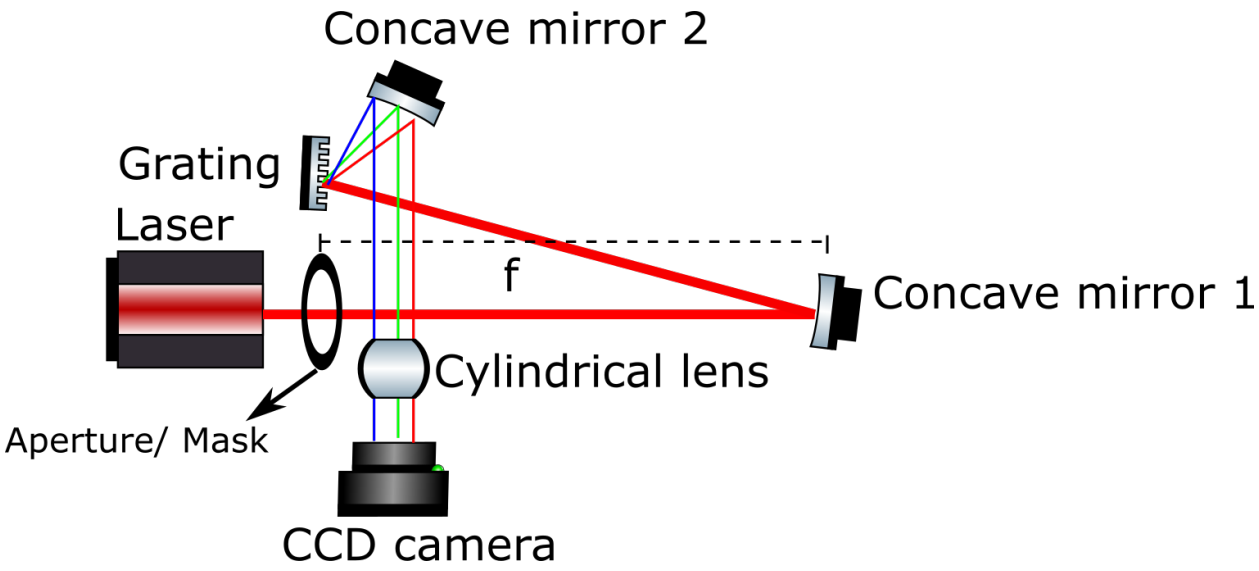

Figure 6: Compact imaging spectrometer, aperture at a distance f to collimate the beam from the concave mirror 1 of focal length f. After hitting the grating, the beam diffracts and reflects onto the concave mirror 2 which focuses the beam into the CCD camera.

3.2 Experimental Setup and Procedure

The schematic of the setup is shown in figure 6. Both the concave mirrors used in this spectrometer had a focal length of 100 mm and the grating constant is 300 groves/mm. To calibrate the spectrometer we used two diode lasers at 405 nm and 450 nm, and a

mask with pin holes separated by 1mm to calibrate the position. The CCD camera (FLIR Grasshopper 3) has a 1" sensor and with a resolution of 3376 * 2704 pixels.

To minimize the astigmatism arising from spherical mirrors, I iteratively adjusted the position of the cylindrical lens and the camera, until we minimize the spot size.

3.3 Results & Observations

3.3.1 Calibration

Figure 7 shows the acquired image using the diode laser of wavelengths 405nm and 450 nm, through the pinhole mask (distance between the slits is 1 mm).

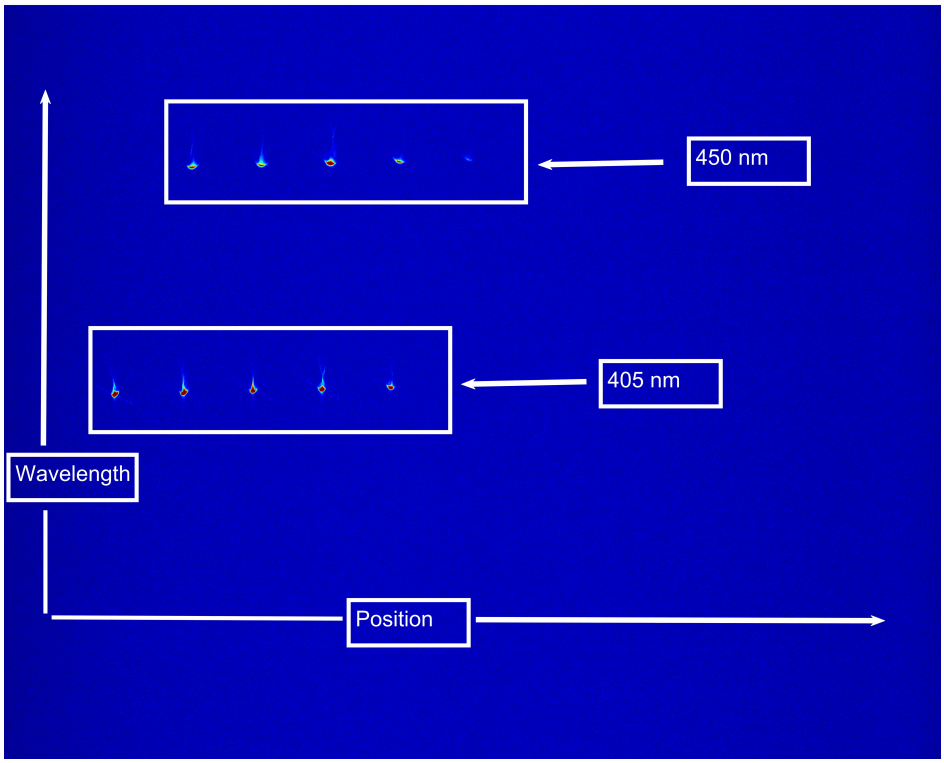

Figure 7: Acquired Image, as discussed before the camera was rotated, hence we observe the wavelength on y-axis and position on x-axis. We can observe the spots from the 405nm and 450nm diode lasers.

The calibrated image is shown in figure 8. From the white and red dashed line which show spots from the 405 nm and 450 nm respectively, there is a little deviation of the spots in wavelengths. This is due to angular orientation of the grating. The spectrometer had a spectral range of 151 nm (330-481 nm) and positional range of 13.5 mm.

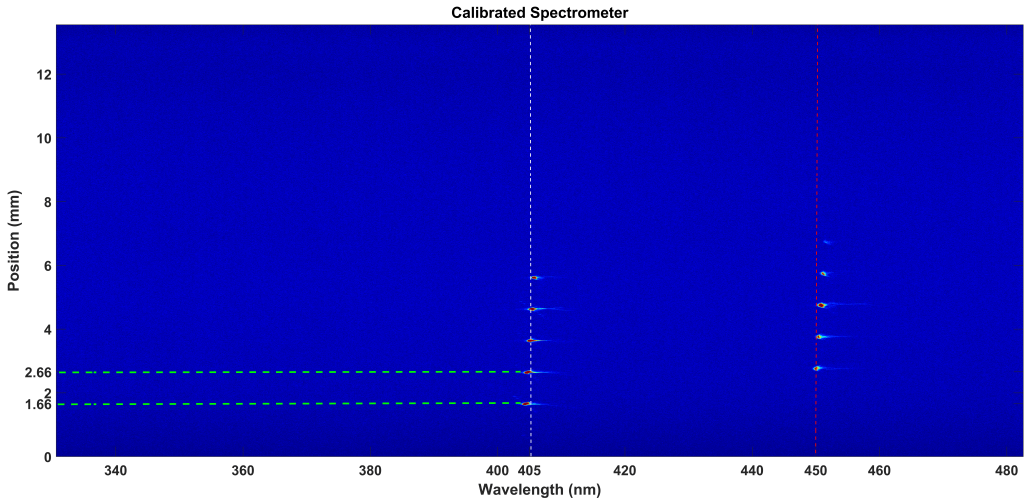

Figure 8: Calibrated Image, white and red dashed line shows spots from the 405 nm and 450 nm respectively. Two green line shows the distance between two spots as 1mm after calibration.

3.3.2 Optimum spot size

From figure 9, we can observe the optimum spot size obtained for the 405 nm spots, this was minimized by using a cylindrical lens. This helps us in achieving optimum imaging quality.

3.3.3 Spectral and spatial resolution

From figure 10(a), the spatial resolution ($\Delta\lambda$) of the spectrometer obtained by averaging the FWHM of the peaks was around 0.6 nm, and from figure 10(b), the spatial resolution obtained by averaging the FWHM of the peaks was around 36 µm.

3.4 Conclusion

We have successfully built and calibrated a compact imaging spectrometer, achieved an optimum imaging quality, which is going to play a huge role in our latest characterization technique. The spectrometer had a spectral range of 151 nm and positional range of 13.5 mm with a spectral resolution of 0.6nm and spatial resolution of 36µm.

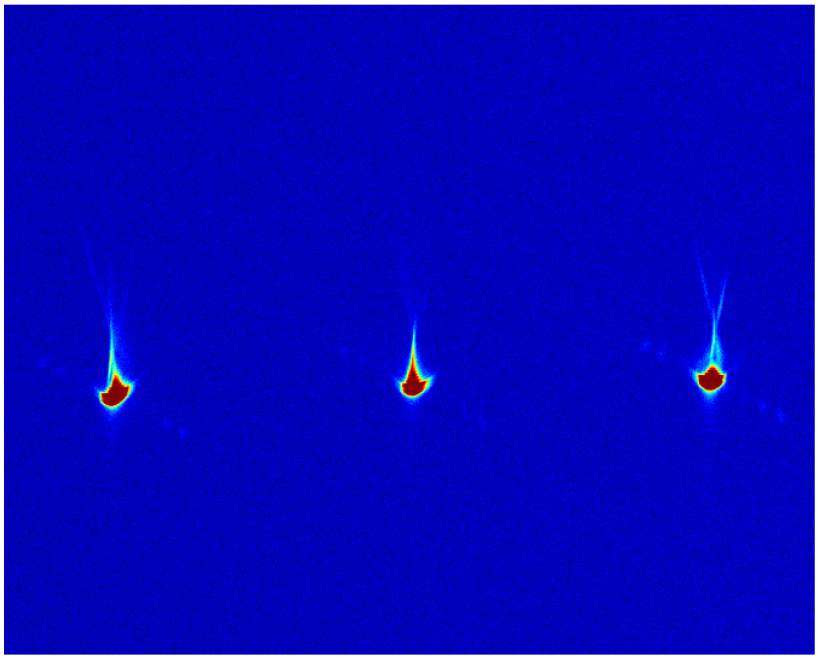

Figure 9: Optimum spot size obtained for the 405nm spots.

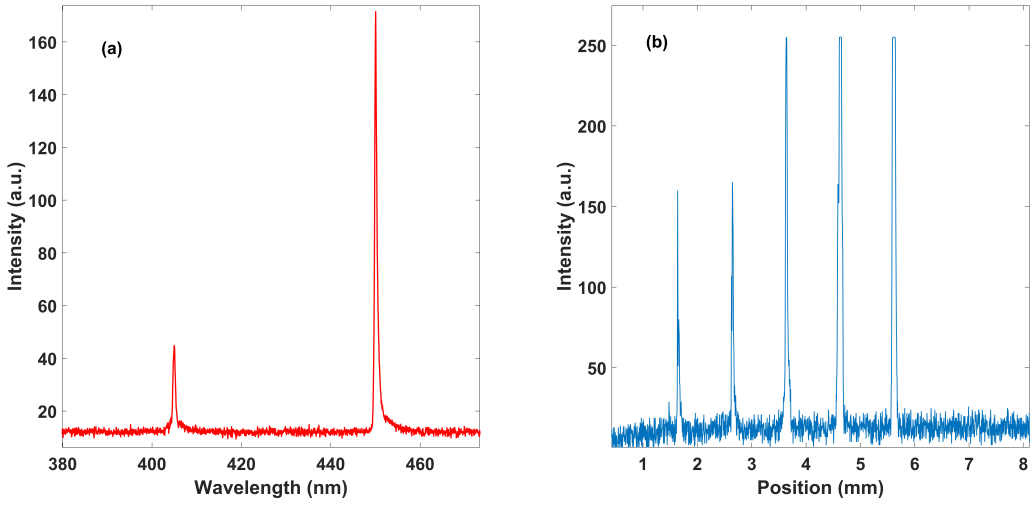

Figure 10: (a) Spectral resolution : Two source peaks obtained by taking average wavelengths around 2.66mm position, and we can observe peaks at 405nm and 450 nm, (b) Spatial resolution:we can observe 5 peaks from the 405nm source.

4 Si-scan (Single Shot D-scan)

4.1 Theory

4.1.1 D-Scan

The ultrashort pulse characterization technique dispersion scan (d-scan) is based on the concept of applying spectral phase on the pulse and recording its SHG spectra as a function of the phase. The d-scan is conceptionally related to the MIIPS technique [7].

Retrieval of spectral phase in MIIPS is obtained by iteratively optimizing the trace until observing a compressed pulse, while in d-scan the phase is retrieved by optimizing the error between the measured and simulated traces.

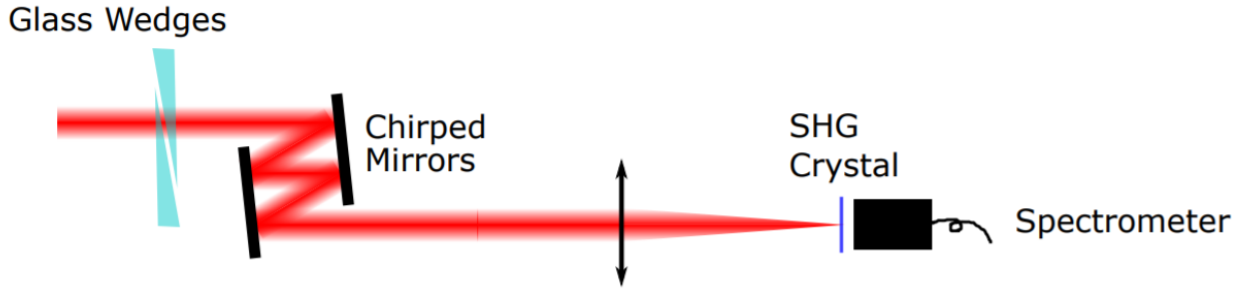

Figure 11: A regular d-scan setup consists of glass wedges to introduce the phase and chirped mirrors introduce negative chirp so that pulse becomes short as possible since glass wedges introduce positive chirp. Generate SH using SHG crystal usually a BBO crystal. Measure the SHG spectrum for different insertion of glass wedges to obtain the 2D d-scan trace from the spectrometer. Image source : [13, p. 22]

The conventional d-scan trace is obtained by varying the spectral phase of the pulse by moving glass wedges as shown in figure (11) and the SHG crystal generates the SH whose spectrum is measured as a function of glass insertion (dispersion). Chirped mirrors in the setup introduce negative chirp so that the pulses can become as short as possible, since glass wedges introduce positive chirp.

The spectral phase function is simply that introduced by linear propagation through a glass, $\varphi(\omega, z)$ = zK(ω), where K(ω) is the glass' wavenumber, and z is the glass' thickness. The SHG spectrum as a function of the glass thickness z is then,

$$I_{trace}(\omega, z) = |\int (\int E(\Omega) e^{izK(\Omega)} e^{i\Omega t} d\Omega)^2 e^{-i\omega t} dt|^2 \tag{9}$$

where $E(\Omega)$ is the complex electric field of the ultrashort laser pulse.

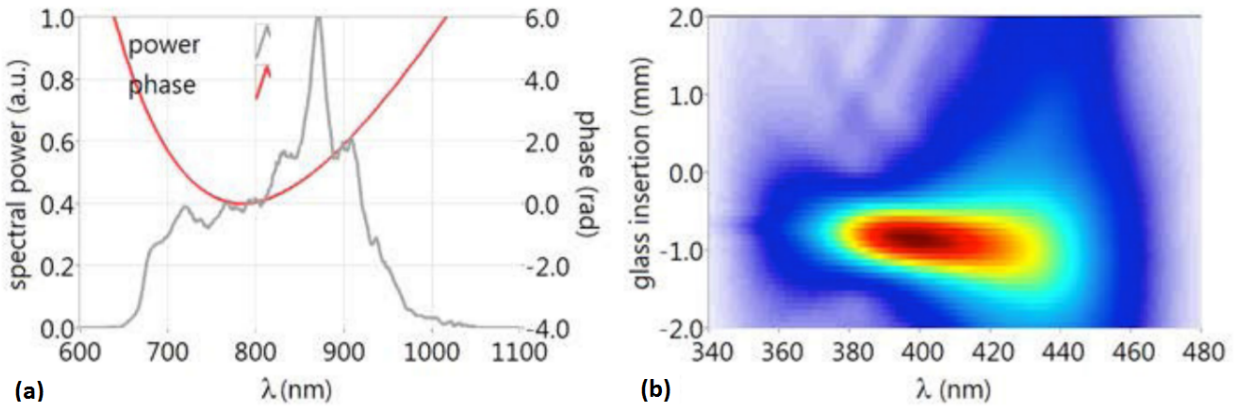

Figure 12: Example of a simulated D-scan trace, (a) spectral plot for zero insertion of the glass wedge, (b) d-scan trace of the spectrum, SHG spectrum as a function of glass insertion (dispersion) . Image source : [14]

A typical d-scan trace is shown in figure 12. It consists of recording the second harmonic spectrum against a known variation of the spectral phase i.e. for different insertions of glass wedges.

The spectral phase of the fundamental pulse can be obtained from the measured d-scan trace by solving an inverse problem iteratively, the retrieval scan is created using the fundamental spectrum and the spectral phase which needs to be obtained. The retrieval algorithm minimize the difference between the measured scan and the retrieved scan by finding the spectral phase [14]. The commonly used phase retrieval algorithms include Nelder-Mead method, Regularization technique for inverse problems, Generalized projections, Differential Evolution, Fast iterative algorithm based on Gerchberg-Saxton algorithm [15, 16].

4.1.2 Single shot D-scan

It is difficult to characterize pulses with low repetition rates using a regular (i.e. scanning) d-scan setup. If there are shot-to-shot fluctuations, the scan using glass wedges would lead to absurd results. To characterize the low repetition pulses we should use a single shot d-scan. A single shot d-scan setup for few-cycle pulses has been demonstrated [8]. It obtains a phase scan by using a prism, where different parts of the beam go through different thickness of the prism and generate SH to obtain the d-scan trace [8].

4.1.3 Compact Single shot D-scan using TSHG crystal (Si-scan)

We introduce the latest characterization technique for low repetition rate laser sources, which is a compact single shot d-scan setup using a TSHG crystal [17]. The TSHG crystal, shown in figure 13, it is a random phase matching nonlinear crystal which introduces dispersion along the crystal and generates the SH in transverse direction. Hence, we obtain a phase scan directly from the crystal, and we can measure the Si-scan trace using a compact imaging spectrometer.

To characterize pulses with longer durations, we need a large dispersion window. In the previous single shot characterization technique where a prism and a BBO crystal, were used the dispersion range was limited. Hence, we use the TSHG crystal which has high dispersion (GDD of around 4800 fs^2 for 10 mm thickness).

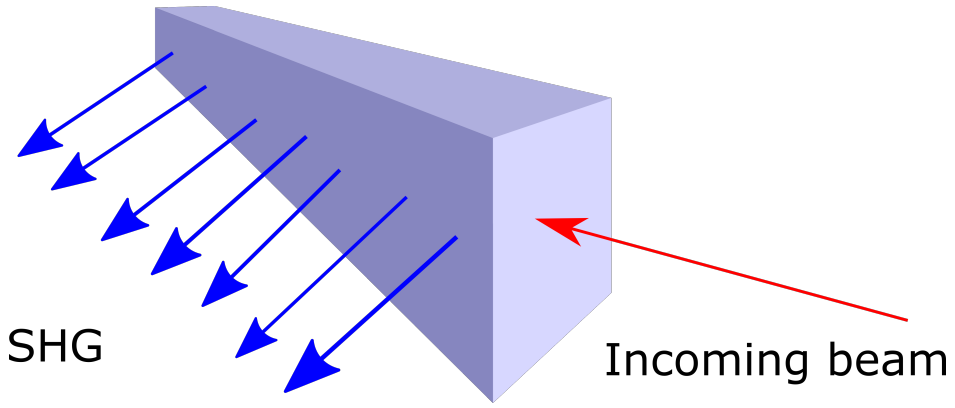

Figure 13: TSHG Crystal, which emits SHG in the transverse direction and introduces dispersion along the crystal.

4.2 Experimental Set-Up and Procedure

Figure 14 shows the setup of our latest characterization technique using a TSHG crystal. The crystal is placed instead of the slit at the focal distance f of concave mirror 1 to collimate the beam into the grating. A laser source with tunable dispersion was used as the driving laser and, it had a wavelength of 800 nm with 1 kHz repetition rate and a maximum pulse energy of 5 mJ.

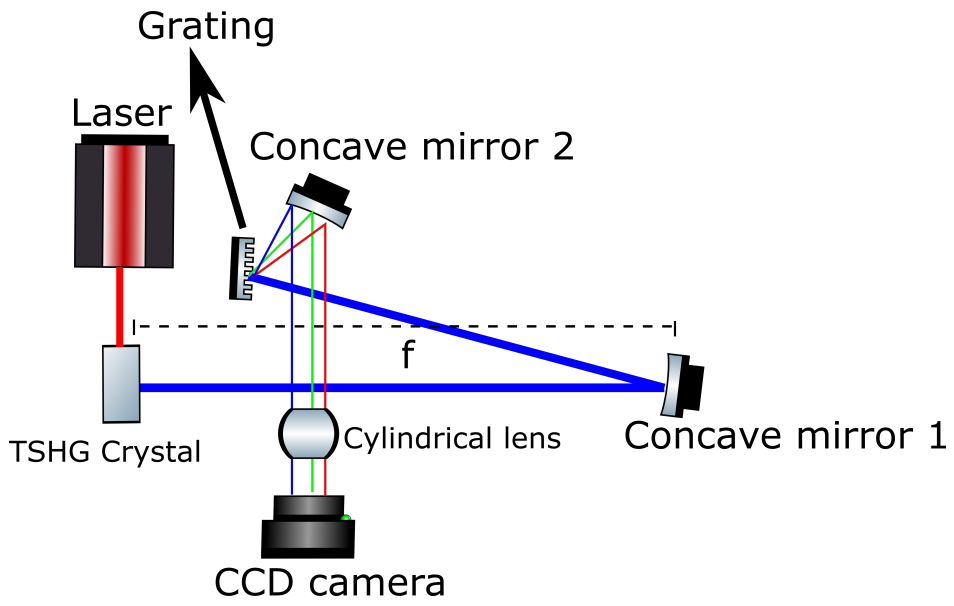

Figure 14: Si-scan setup, incoming beam (red) generates SHG (blue) with dispersion in transverse direction, the scan is recorded by imaging spectrometer.

4.3 Results & Observations

From figure 15 (a), we could see the measured Si-scan trace and figure 15 (b) shows the retrieved Si-scan trace obtained from fast retrieval algorithm, the measured and retrieved scan look quite similar except that the measured scan has little high intensity away from the center compared to the retrieved scan. This could be due to some nonlinear behaviour of the crystal in the non-transverse directions, adding noise to our SH signal.

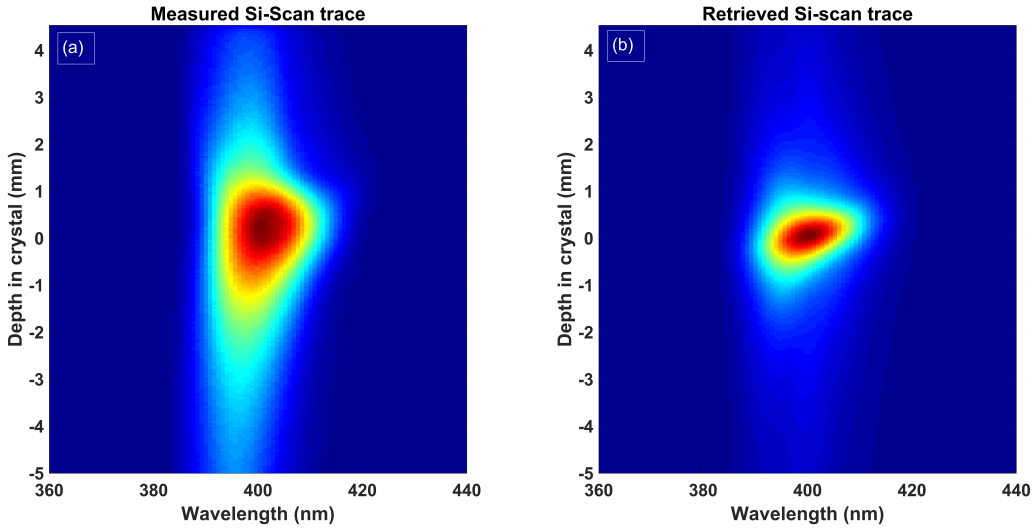

Figure 15: Measured (a) and Retrieved (b) Si-scan trace, SHG spectrum as as function of depth in crystal i.e. dispersion introduced by the crystal.

The retrieved pulse in the spectral domain can be seen from figure 16 (a) which is obtained at zero depth i.e. at maximum compression in crystal from figure 15 (b), and 16 (b) shows the retrieved pulse in the time domain with a pulse duration of about 23 fs, which is quite close to the Fourier limit for pulses with a 100 nm bandwidth centered around 800 nm.

There were no chirped mirrors in the setup to introduce negative dispersion. The dispersion of the laser can be tuned by a programmable acousto-optic dispersion filter. Reducing second-order dispersion by about 2000 fs^2, centered the trace in the crystal. The center mass of the scan is almost at the center of the crystal, by varying the GDD, we observed that the center of mass of the scan was shifted along the crystal depth. This gives us immediate response about our laser system from the scan traces, and it could be helpful in optimizing our setup without retrieval.

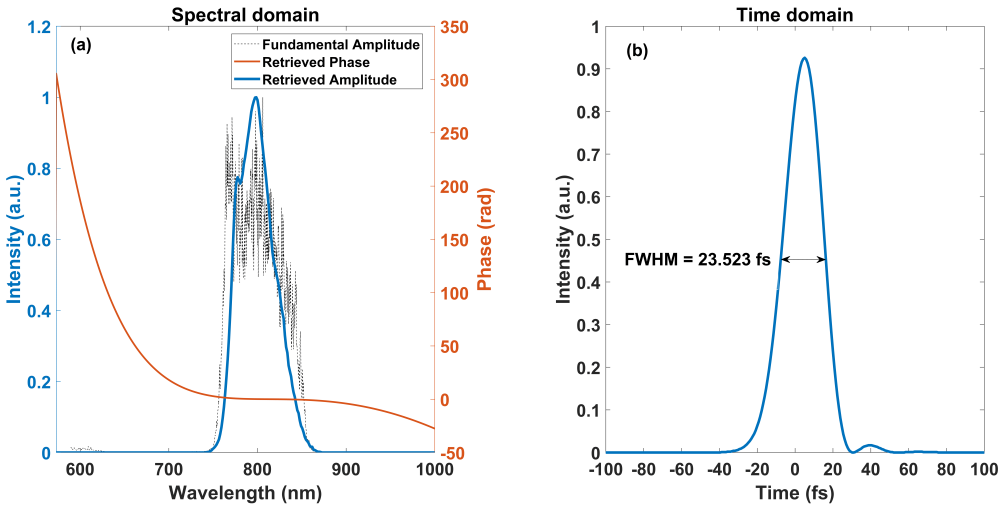

Figure 16: Retrieved pulse at zero depth from retrieved Si-scan trace, (a) Black shows the fundamental spectrum amplitude, blue shows the retrieved spectral amplitude, red shows the retrieved spectral phase (b) Retrieved pulse construction in time domain, it has a pulse duration of about 23 fs

4.4 Conclusion

We have successfully implemented a new compact single shot pulse characterization technique using a TSHG crystal, successfully characterized our laser source and the pulse duration was found to be around 23 fs. This technique can also be used to characterize even pulses with broader spectral range and shorter durations, and this is due to high dispersion of the crystal (GDD variation of almost 4800 fs^2 over 10 mm thick TSHG crystal).

Si-scan trace without retrieval gives us immediate indication about the laser system which could be helpful to optimize our setup.

Retrieving the Si-scan was still challenging, since we do not completely understand the non linear properties of the crystal. We could improve the trace by using some filters to filter out the beam coming from other parts (non transverse direction) of the crystal.

5 White light generation

One of the aim is to explore the d-scan at different wavelengths, for example we have a Pharos laser source at 1030nm with a pulse duration of 170 fs. Introducing sufficiently much dispersion is more challenging for longer pulses. Therefore, we need shorter pulses (< 40 fs) in-order to test the d-scan. We make to use of nonlinear techniques to obtain such short pulses. In this work we use white light generation in a crystal to achieve short pulses. We study the white-light at different generation conditions, including the effect of focal lens (lens used to focus the light into the crystal), laser power, crystal thickness, so that we can obtain a sufficiently broadened spectrum supporting 20 fs pulses.

5.1 Theory

White light generation (WLG), also known as supercontinuum generation is a phenomenon of nonlinear optics where the pulse's spectrum is broadened. WLG can take place when a powerful ultrashort laser pulse is focused into a crystal. Despite being widely used, the mechanism is still under study. The primary factors resulting in WLG are believed to be the optical Kerr effect and Multi Photon Ionization (MPI) induced plasma [18]. Some of the applications of supercontinuum sources are spectral interferometry, time resolved absorption/excitation spectroscopy, optical pulse compression etc.. [19]

Supercontinuum generation is usually explained by nonlinear light-matter interaction. Nonlinear optics is a field of optics which describes the behaviour of light in nonlinear media. It occurs as a consequence of the alteration of the optical properties of a material by the presence of light, where the polarization density ($\overline{P}$) is non-linearly related to the electric field ($\overline{E}$) of the light. Equation (10) shows the relation between polarization density and electric field of the light in linear media. The modified representation of the Taylor series expansion of equation (10) is shown in equation (11), which gives us the relation between polarization density and electric field of the light in nonlinear media, where ϵ_o is the permittivity in vacuum and $\chi^{(n)}$ is the nth order optical susceptibility of the medium. [20, p. 876]

$$\overline{P} = \epsilon_o \chi \overline{E} \tag{10}$$

$$\overline{P} = \epsilon_o \chi \overline{E} + 2\epsilon_o \chi^{(2)} \overline{E}^2 + 4\epsilon_o \chi^{(3)} \overline{E}^3 + ... \tag{11}$$

Let the electric field E(t) of light be as shown in equation 12, where E_o is the complex envelope in the temporal domain and E_o^* is its complex conjugate. From equation 13, we can see that the term $E(t)^2$ leads to the generation of second harmonic (2ω), similarly nonlinearity can lead to generation of new frequency components from the equation 11. [20, p. 876]

$$E(t) \propto E_o exp(j\omega t) + E_o^* exp(-j\omega t) \tag{12}$$

$$E(t)^2 \propto E_o^2 exp(j(2\omega)t) + 2|E_o|^2 + E_o^{*2} exp(-j(2\omega)t) \tag{13}$$

5.1.1 Optical Kerr effect

The Optical Kerr effect relates to the change in refractive index of a medium due to the electric field of the incident light. What John Kerr discovered is the DC Kerr effect [21]. We use the AC Kerr effect here. A medium with centrosymmetry, i.e. it contains an inversion center, second order susceptibility is not present ($\chi^{(2)}$=0), so that the third order susceptibility ($\chi^{(3)}$) becomes dominant. Such materials are also called Kerr media.

As discussed above the refractive index becomes intensity dependent, and the relation between the intensity and refractive index of the material is given by equation (14), where n is the linear refractive index and n_2 is given in equation (15). [20, p. 895-896]

$$n(I) = n + n_2 I \tag{14}$$

$$\text{where } n_2 = \frac{3}{4n^2 c\epsilon_o}\chi^{(3)} \tag{15}$$

5.1.2 Self-phase modulation (SPM)

Ultrashort laser pulses travelling through a medium will induce a varying refractive index due to the Optical Kerr effect as discussed above and this change in refractive index will create a time-dependent phase shift in the pulse, i.e. the pulse experiences an intensity dependent phase shift and this leads to spectral broadening of the pulse.[22, 23]

Let I(z,t) be the intensity profile of the laser beam in space and time. The phase shift introduced by the Kerr effect is given by equation (16), where L is the distance travelled in the medium, and k is the propagation wave number. The instantaneous frequency ($\omega(t)$)

is given by equation (17) and we can see that the generation of new frequencies depends on the slope of the pulse $\partial I(z,t)/\partial t$.

$$\Delta\phi(t) = \int_0^L -n_2 I(z,t) k dz \tag{16}$$

$$\omega(t) = -\frac{\partial\phi(t)}{\partial t} = \omega_o - n_2 \frac{\partial I(z,t)}{\partial t} kz \tag{17}$$

5.1.3 Self-steepening

Self steepening is the consequence of Optical Kerr effect. In the temporal domain the central part of the pulse has higher intensity and therefore it experiences higher refractive index (eq 15) compared to the edges. The central part travels slowest and because of that the trailing edge runs into the peak. As a consequence the trailing edge becomes steeper, which promotes the generation of blue-shifted frequencies.

5.1.4 Self-focusing

In the spatial domain, the intensity is higher at the center of the beam compared to the edges and this leads to higher refractive index in the medium, which leads to a spatial curvature that acts as focusing lens for the beam. Self focusing in a nonlinear Kerr medium is illustrated in figure (17). The peak power of the pulse should be higher than the critical power (P_c) in order for the self focusing to occur. The critical power (P_c) is given by equation (18), where α_t is a constant, which depends on the shape of the pulse and it is approximately 1.8962 for Gaussian beam shape [23].

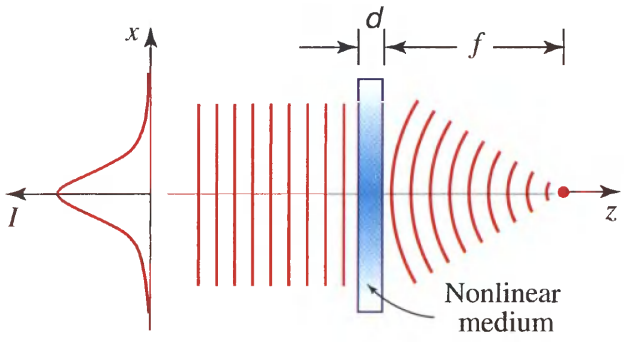

Figure 17: Self focusing effect, where nonlinear Kerr medium acts as lens. Image Source : [20, p. 897]

$$P_c = \frac{\alpha_t \lambda^2}{4\pi n n_2} \tag{18}$$

5.1.5 Multi-Photon Ionization (MPI)

The high intensity of the light may lead to ionization of the medium, i.e. several absorbed photons with energy below ionization threshold. The probability of ionization is proportional to I^k, where I is the intensity and k is the ionization order, i.e. the number of photons needed to overcome the ionization potential. Hence the higher the intensity, the higher the probability of ionization. At intensities high enough to generate a considerable amount of free electrons, the resulting plasma exhibits a lower refractive index than that of the neutral medium. The sudden drop of refractive index promotes spectral broadening on the blue side.

5.1.6 Plasma defocusing

As the intensity is higher in the center of the beam compared to the edges, so is the ionization more probable and the refractive index lower. This creates an effect opposite to self-focusing, called plasma defocusing.

5.1.7 Filamentation

Due to self-focusing the beam spatially contracts. As the intensity grows, MPI sets in and a plasma is formed. In the following a dynamic balance between self-focusing and plasma-defocusing is established, stabilizing the beam at small diameter for distances much longer than the respective Rayleigh range. This is called filamentation. The process is illustrated in figure (18). During filament formation, spectral broadening occurs due to several nonlinear phenomena, such as SPM, self steepening, self focusing, MPI and plasma defocusing.

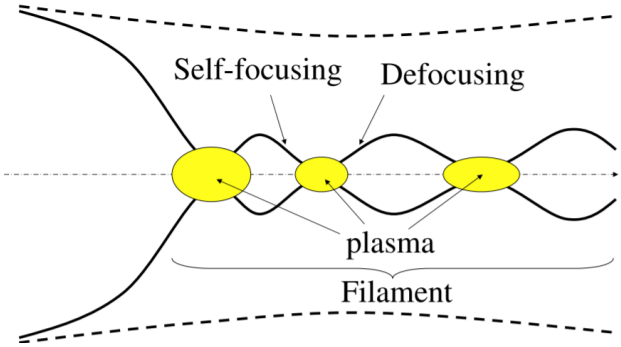

Figure 18: Filamentation generated in the medium, Self focusing ionizes the medium creating MPI which leads to plasma defocusing, This process repeats many times and it is usually around few millimeters long. Image source : [18, p. 57]

5.2 Experimental Setup and Procedure

The source used in the experiment was a PHAROS a high power femtosecond laser system, which is based on Chirped Pulse Amplification (CPA). The Source has a central wavelength of 1030 nm, it delivers pulse duration of 150 -250 fs, 5 μJ of energy per pulse at a repetition rate of 200 kHz. The repetition rate, pulse duration and pulse energy were tunable.

The experiment is shown in figure 19. The laser beam was focused into a YAG (yttrium aluminium garnet) crystal by a convex lens. An attenuator which consists of a half-wave plate and a polarizer was used to vary the power. The generated white light was analyzed by the OSA. We begin by varying the power by using attenuator until we observe white light physically, and than look at the spectrum to make sure there is no spectral modulations, which will be discussed in section 5.3.2.

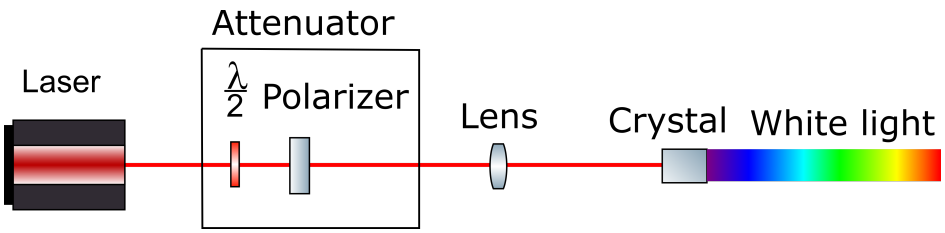

Figure 19: Setup for white light generation.

5.3 Results & Observations

Figure 20 shows the setup and the generated white-light can be observed on the aperture, which was obtained using a 4 mm thick YAG crystal and a convex lens of 60 mm focal length. We have also used an 8 mm thick YAG crystal and a convex lens with 125 mm focal length.

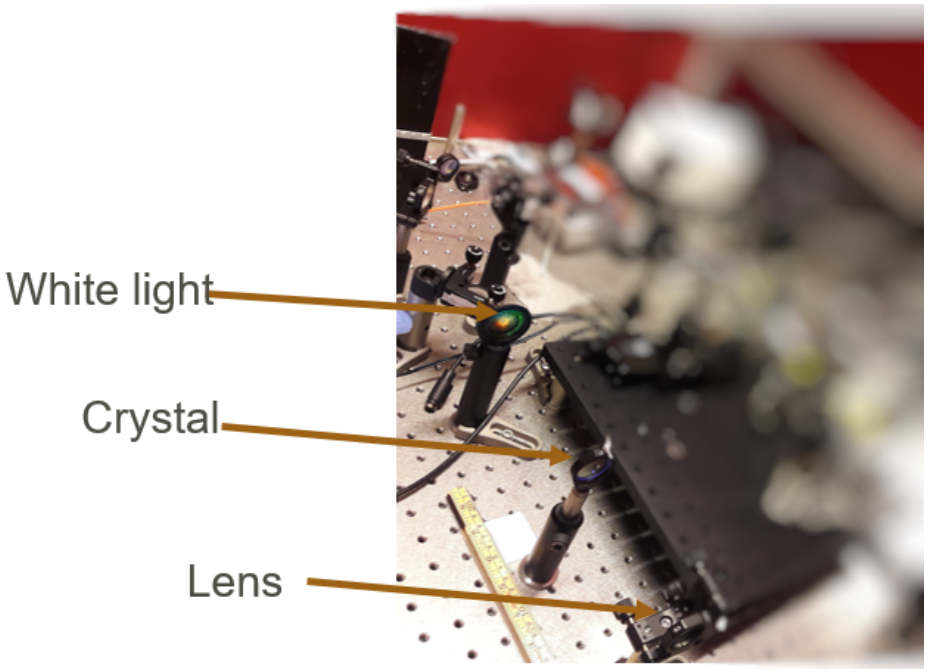

Figure 20: Generated white-light can be observed on the aperture, which was obtained using 4mm thick YAG crystal and convex lens of 60mm focal length.

5.3.1 Effect of focal length

From the experimental setup one can see that the convex lens of focal length f is used to focus the laser pulse into the YAG crystal. Suppose the beam size before focus was W_o, the beam size after passing through the lens at the focus would be W' given by equation (19). The focal length of the lens is proportional to the beam size (spot size), hence using long focal length leads to increased beam size. The wave-front of the beam experienced by the crystal is different for each focal lengths, hence they experience different Kerr effect, which effects the white light generation.

From figure (21), we can observe that the spectrum is slightly broader for the 60 mm focal length compared to the 125 mm focal length. From equation (19), we can see that the

125 mm focal length has larger beam size focused at the crystal compared the 60 mm focal length. The laser pulses can propagate only several centimetres in the medium before they collapse, this is called as collapse/filamentation distance. The filamentation distance is proportional to the beam size, to achieve highly efficient white light the collapse distance should be small [24, 25].

$$W' = \frac{\lambda}{\pi W_o} f \tag{19}$$

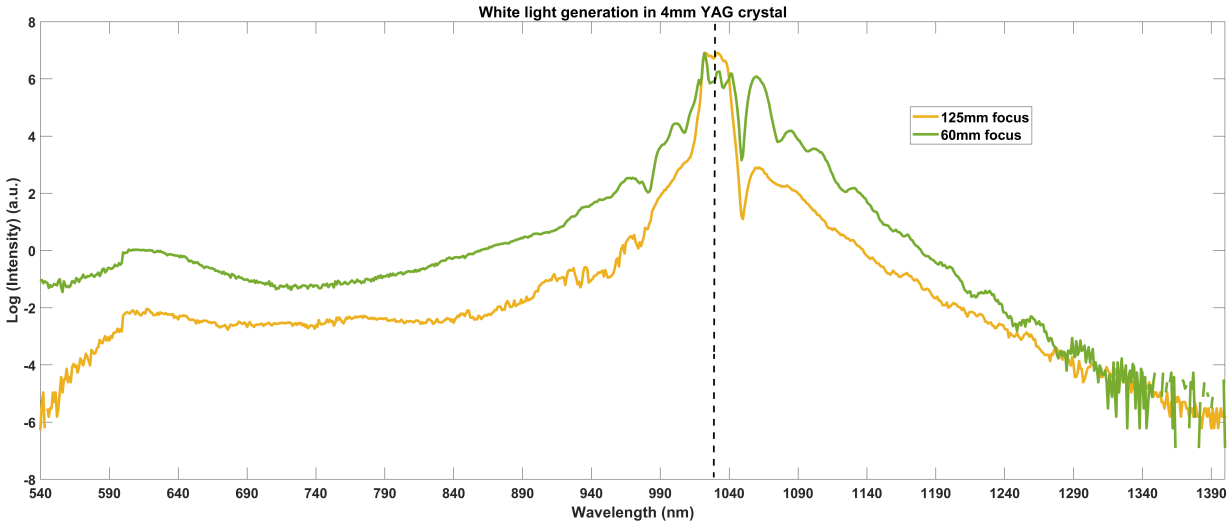

Figure 21: Effect of focus on 4mm YAG crystal. The green spectrum (focal length 60mm) has slightly broader spectrum compared to the yellow spectrum (focal length 125mm). The dashed line shows the wavelength of the fundamental spectrum (1030 nm).

5.3.2 Effect of power

The critical power for YAG is 1.36 MW [26]. We have to focus with power higher than the critical power to generate white light. From figure (22), we can observe the fluctuations in spectrum, when we focus with too high power. This could be due to the splitting of pulse in the time domain, which would manifest as a modulated spectrum (spectral interference).

5.3.3 Effect of crystal thickness

From spectrum figure (23), we can observe that 4 mm and 8 mm crystal generate nearly the same. This could be due to saturation of the spectrum broadening inside the medium

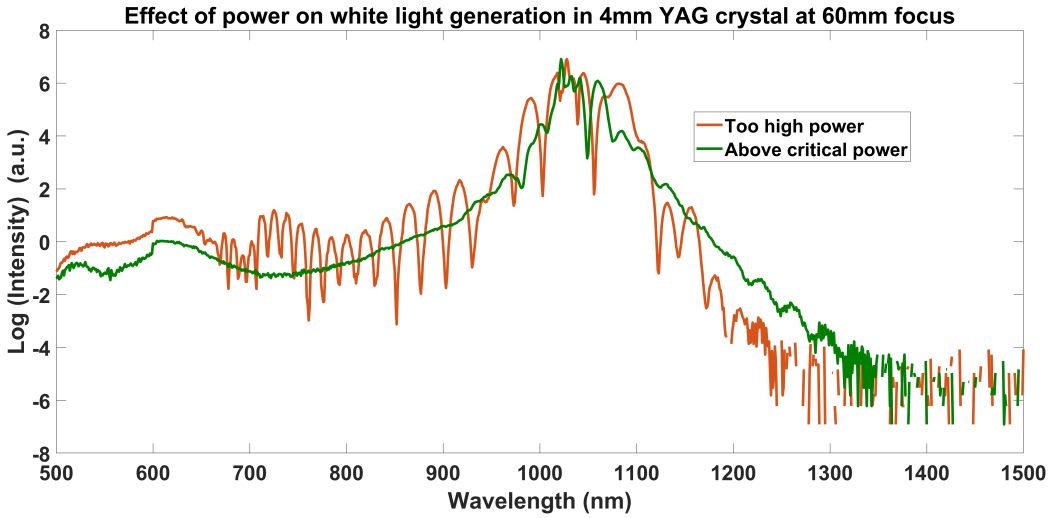

Figure 22: Effect of Power on 4mm YAG crystal by using 60mm focal length. Too high power leading to oscillations in the spectrum (orange spectrum).

after propagating some distance.

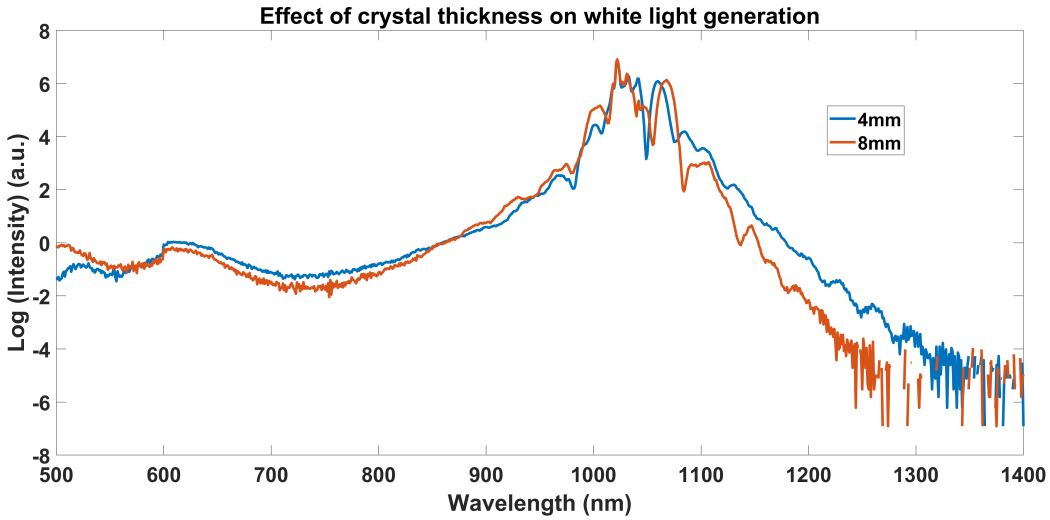

Figure 23: Effect of YAG crystal thickness on white light generation, by using 60mm focal length.

5.4 Conclusion

The main goal was to generate efficient white light, so we could verify whether the characterization technique (D-scan) works for broader spectral range. The final configuration obtained for generating efficient white light is by using a 4 mm/8 mm YAG crystal, con-

vex lens of 60 mm focal length and power just above critical power. From the theory the generation should be higher towards blue frequencies and we could observe from the measurements that it was in agreement. Obtaining highly efficient broadening towards higher wavelengths is still challenging.

6 Conclusion & Outlook

The main goal of this thesis was to implement a new compact characterization technique (Si-scan) for ultrashort laser pulses, and it was successfully implemented. This was achieved by using a TSHG crystal which played an import role in generating the Si-scan trace, by introducing dispersion as well as generating SHG.

The white light spectral interferometry technique to measure the dispersion properties of material was discussed in section 2, which included a phase extraction algorithm for retrieving the spectral phase introduced by the material. Dispersion properties of this random phase matching TSHG crystal were obtained by using white light spectral interferometry. The GVD of the TSHG crystal was around 480 fs^2/mm, which was quite high compared to the glass wedges/prisms used in previous characterization techniques, which would be helpful in characterizing pulses narrower spectrum and longer durations. Too large delay made it difficult to extract the dispersion of the material, since the interference fringes were quite dense, which makes it difficult to filter the sideband in the time domain.

A compact imaging spectrometer (crossed Czerny-Turner imaging spectrometer) for Si-scan was built and calibrated according to our scanning requirements, which played a huge role in making this whole setup really compact. It was astigmatism free and had a broad spectral range with sufficient spectral and spatial resolution.

Retrieving the Si-scan remained challenging. We could improve the trace by using filters to block scattered light.

Some of the future work would be to improve the signal from the TSHG crystal. Implementing deep learning model to optimize the d-scan retrieval algorithm and retrieve the trace more accurate and quickly. Vary the power and observe the traces, since SHG from TSHG crystal depends on the power, this could help us in finding the optimum power to improve the Si-scan trace.

The Si-scan can be an important device for continuous monitoring of a femtosecond laser. A change of dispersion, e.g. induced by heating compressor gratings, would result in a shift of the d-scan trace, easy to detect without retrieval.

Extending the Si-scan technique to different wavelengths would be one of the next steps. The efficiency of second harmonic generation as function of wavelength would need to be characterized. The TSHG crystal becomes absorbing below 350 nm, which limits the usability for fundamental pulses below 750 nm central wavelength. The imag-

ing spectrometer would not be a problem for recording the traces, since we can adjust our design according to our spectral range needs.

Extending the Si-scan technique for different pulse durations, for shorter pulse durations (<20 fs), we have to have better resolution along the depth for our imaging spectrometer, since it requires less dispersion. For longer pulse durations (>20 fs), we need high dispersion and hence we need to use longer crystals, and this would be challenging to image, we need to adjust our imaging spectrometer design and might have to use larger optical components and CCD camera with lager sensor, our design might not be compact anymore.

References

[1] M. Miranda. "Sources and Diagnostics for Attosecond Science". eng. PhD thesis. Lund University, 2012, p. 218. ISBN: 978-91-7473-392-1.

[2] Daimler. *Mercedes AMG Petronas Motorsport unveiled its car for the 2017 season at Silverstone, England*. WIRED, Feb. 2017. URL: https://www.wired.com/2017/02/f1s-funky-new-cars-promise-faster-exciting-racing/.

[3] A. H. Zewail. "Laser femtochemistry". In: *Science* 242.4886 (1988), pp. 1645–1653.

[4] T. Oksenhendler. "Self-referenced spectral interferometry theory". In: *arXiv preprint arXiv:1204.4949* (2012).

[5] C. Iaconis and I. A. Walmsley. "Spectral phase interferometry for direct electric-field reconstruction of ultrashort optical pulses". In: *Optics letters* 23.10 (1998), pp. 792–794.

[6] D. J. Kane and R. Trebino. "Characterization of arbitrary femtosecond pulses using frequency-resolved optical gating". In: *IEEE Journal of Quantum Electronics* 29.2 (1993), pp. 571–579.

[7] V. V. Lozovoy, I. Pastirk, and M. Dantus. "Multiphoton intrapulse interference.IV.Ultrashort laser pulse spectral phase characterization and compensation". In: *Opt. Lett.* 29.7 (Apr. 2004), pp. 775–777. DOI: 10.1364/OL.29.000775.

[8] M. Louisy et al. "Compact single-shot d-scan setup for the characterization of few-cycle laser pulses". In: *Appl. Opt.* 56.32 (Nov. 2017), pp. 9084–9089. DOI: 10.1364/AO.56.009084.

[9] S. Diddams and J.-C. Diels. "Dispersion measurements with white-light interferometry". In: *JOSA B* 13.6 (1996), pp. 1120–1129.

[10] V. Messager et al. "Coherent measurement of short laser pulses based on spectral interferometry resolved in time". In: *Opt. Lett.* 28.9 (May 2003), pp. 743–745. DOI: 10.1364/OL.28.000743.

[11] I. H. Malitson.
"Interspecimen Comparison of the Refractive Index of Fused Silica∗,†".
In: *J. Opt. Soc. Am.* 55.10 (Oct. 1965), pp. 1205–1209. DOI: 10.1364/JOSA.55.001205.

[12] Y. An et al. "The design of astigmatism-free crossed Czerny-Turner spectrometer".
In: *Optik* 124.16 (2013), pp. 2539–2543.

[13] C. Guo. "A High Repetition Rate Attosecond Light Source Based on Optical Parametric Amplification". eng. PhD thesis. Lund University, 2018.
ISBN: 978-91-7753-558-4.

[14] M. Miranda et al. "Simultaneous compression and characterization of ultrashort laser pulses using chirped mirrors and glass wedges".
In: *Opt. Express* 20.1 (Jan. 2012), pp. 688–697. DOI: 10.1364/OE.20.000688.

[15] E. Escoto et al.
"Advanced phase retrieval for dispersion scan: a comparative study".
In: *J. Opt. Soc. Am. B* 35.1 (Jan. 2018), pp. 8–19. DOI: 10.1364/JOSAB.35.000008.

[16] M. Miranda et al. "Fast iterative retrieval algorithm for ultrashort pulse characterization using dispersion scans".
In: *J. Opt. Soc. Am. B* 34.1 (Jan. 2017), pp. 190–197. DOI: 10.1364/JOSAB.34.000190.

[17] R. Fischer et al. "Broadband femtosecond frequency doubling in random media".
In: *Applied Physics Letters* 89.19 (2006), p. 191105. DOI: 10.1063/1.2374678.
eprint: https://doi.org/10.1063/1.2374678.

[18] A. Couairon and A. Mysyrowicz.
"Femtosecond filamentation in transparent media".
In: *Physics reports* 441.2-4 (2007), pp. 47–189.

[19] R. Dorsinville et al. "Applications of Supercontinuum: Present and Future".
In: *The supercontinuum laser source*. Springer, 1989, pp. 377–398.

[20] M. T. B.E.A. Saleh. *Fundamentals of Photonics. (second edition)*. Wiley, 2007.

[21] J. K. LL.D. "XL. A new relation between electricity and light: Dielectrified media birefringent". In: *The London, Edinburgh, and Dublin Philosophical Magazine and Journal of Science* 50.332 (1875), pp. 337–348. DOI: 10.1080/14786447508641302.
eprint: https://doi.org/10.1080/14786447508641302.

[22] R. R. Alfano and S. Shapiro. “Observation of self-phase modulation and small-scale filaments in crystals and glasses”.
In: *Physical Review Letters* 24.11 (1970), p. 592.

[23] A. Brodeur and S. Chin. “Ultrafast white-light continuum generation and self-focusing in transparent condensed media”.
In: *JOSA B* 16.4 (1999), pp. 637–650.

[24] S. Eisenmann et al. “Control of the filamentation distance and pattern in long-range atmospheric propagation”.
In: *Opt. Express* 15.6 (Mar. 2007), pp. 2779–2784. DOI: 10.1364/OE.15.002779.

[25] M. Kolesik, D. E. Roskey, and J. V. Moloney. “Conditional femtosecond pulse collapse for white-light and plasma delivery to a controlled distance”.
In: *Opt. Lett.* 32.18 (Sept. 2007), pp. 2753–2755. DOI: 10.1364/OL.32.002753.

[26] A.-L. Calendron et al. “White-light generation with sub-ps pulses”.
In: *Opt. Express* 23.11 (June 2015), pp. 13866–13879. DOI: 10.1364/OE.23.013866.

[27] T. Gaumnitz et al. “Streaking of 43-attosecond soft-X-ray pulses generated by a passively CEP-stable mid-infrared driver”.
In: *Opt. Express* 25.22 (Oct. 2017), pp. 27506–27518. DOI: 10.1364/OE.25.027506.